

From Words to Wavelengths: VLMs for Few-Shot Multispectral Object Detection

Manuel Nkegoum^{1,3}, Minh-Tan Pham¹, Élisabeth Fromont², Bruno Avignon³ and Sébastien Lefèvre^{1,4}

¹Univ Bretagne Sud, IRISA, UMR 6074, Vannes, France

²Univ Rennes, IRISA, UMR 6074, Rennes, France

³ATERMES, Montigny-le-Bretonneux, France

⁴UiT The Arctic University of Norway, Tromsø, Norway

{manuel.nkegoum-nzouakeu,minh-tan.pham,elisa.fromont,sebastien.lefevre}@irisa.fr,
bavignon@atermes.fr

Abstract

Multispectral object detection is critical for safety-sensitive applications such as autonomous driving and surveillance, where robust perception under diverse illumination conditions is essential. However, the limited availability of annotated multispectral data severely restricts the training of deep detectors. In such data-scarce scenarios, textual class information can serve as a valuable source of semantic supervision. Motivated by the recent success of Vision-Language Models (VLMs) in computer vision, we explore their potential for few-shot multispectral object detection. Specifically, we adapt two representative VLM-based detectors, Grounding DINO and YOLO-World, to handle multispectral inputs and propose an effective mechanism to integrate text, visual and thermal modalities. Through extensive experiments on two popular multispectral image benchmarks, FLIR and M3FD, we demonstrate that VLM-based detectors not only excel in few-shot regimes, significantly outperforming specialized multispectral models trained with comparable data, but also achieve competitive or superior results under fully supervised settings. Our findings reveal that the semantic priors learned by large-scale VLMs effectively transfer to unseen spectral modalities, offering a powerful pathway toward data-efficient multispectral perception.

1. Introduction

Reliable perception under adverse conditions such as nighttime, fog, or occlusion is essential for safety-critical systems in autonomous driving, surveillance, and robotics. Multispectral object detection addresses this challenge by leveraging complementary information from visible (RGB)

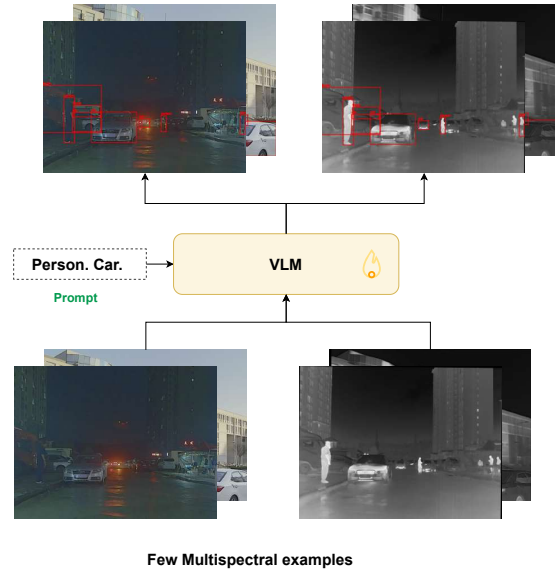


Figure 1. Conventional multispectral detectors require many annotated, aligned RGB-IR pairs for training. Our approach leverages the semantic priors of vision-language models (VLMs) to bridge this data gap. Given only a few labeled multispectral examples and a text prompt (e.g., “person, car, bicycle”), the adapted VLM can robustly detect objects across spectral domains by jointly reasoning over visual (RGB) and thermal (IR) cues.

and infrared (IR) modalities, enabling robust detection even when one modality degrades. However, the widespread adoption of multispectral detectors remains limited by the scarcity of large-scale annotated data, as collecting and aligning multispectral image pairs with precise bound-

ing boxes is time-consuming. Recent progress in vision-language models (VLMs) has revolutionized few-shot and open-vocabulary object detection in the RGB domain [11, 13]. By jointly learning from vast amounts of image–text pairs, these models acquire rich semantic priors that allow them to recognize novel concepts with minimal supervision (see Fig. 1). Such capabilities naturally raise a fundamental question: *Can the semantic grounding learned by VLMs in the RGB domain transfer to multispectral settings, thereby mitigating the need for large labeled datasets?*

In this work, we explore this question through an extensive empirical study of VLM-based detectors for *few-shot multispectral object detection*. Rather than introducing a completely new architecture, we adapt two representative VLM frameworks—Grounding DINO [11] (GDINO) and YOLO-World [2] (YOLOW)—to operate on multispectral inputs with minimal modification. This allows us to isolate and analyze the impact of large-scale semantic pre-training on multispectral generalization. Our study yields several key findings. First, we show that VLM-based detectors are surprisingly strong few-shot learners in the multispectral domain, significantly outperforming existing specialized methods trained with comparable data. Second, we observe that, even in fully supervised regimes, these adapted VLMs achieve or surpass state-of-the-art performance, suggesting that semantic grounding not only aids data efficiency but also improves general robustness across modalities. Finally, our analysis reveals that simple fusion strategies, when coupled with semantically informed representations, are sufficient to unlock strong cross-spectral transfer without requiring complex architectural changes. In summary, our contributions are threefold:

1. We present the first systematic investigation of VLMs for few-shot multispectral object detection, establishing a new experimental framework and strong baselines.
2. We propose suitable adaptations of Grounding DINO and YOLO-World to handle multispectral inputs, demonstrating that semantic grounding effectively transfers across spectral modalities.
3. We achieve state-of-the-art results on FLIR and M3FD datasets in both few-shot and fully supervised settings, highlighting the promise of VLMs as data-efficient multispectral learners.

2. Related Work

2.1. Object Detection

Object detection has witnessed remarkable progress driven by deep learning architectures. Two-stage detectors like Faster R-CNN [18] pioneered region proposal mechanisms followed by classification and regression. Subsequent one-stage approaches including YOLO [17] and SSD [12] achieved improved efficiency through unified prediction

frameworks. More recently, transformer-based detectors such as DINO [26] and RT-DETR [27] have demonstrated superior performance by leveraging self-attention mechanisms and dynamic object queries. Collaborative frameworks like Co-DETR [28] further enhanced detection performance through multi-view supervision and auxiliary training signals. These architectural advances have established a solid foundation for high-performance object detection, providing the building blocks for multispectral extensions.

2.2. Multispectral Object Detection

Multispectral object detection exploits complementary information from different imaging modalities to enhance robustness under challenging conditions. Early fusion approaches simply concatenated features from different spectra, while more sophisticated methods developed specialized fusion strategies. GAFF [25] introduced Guided Attentive Feature Fusion with inter- and intra-modality attention mechanisms to dynamically combine multispectral features. CAFF-DINO [6] incorporated cross-attention feature fusion within a transformer framework, effectively handling misaligned image pairs. DAMSDet [5] proposed a Dynamic Adaptive Multispectral Detection Transformer with modality-competitive query selection and deformable cross-attention for adaptive fusion. Most recently, GM-DETR [21] enhanced global context modeling across spectral channels, improving detection consistency across varying illumination conditions. These methods collectively demonstrate that sophisticated cross-modal interaction strategies are essential for high-performance multispectral detection.

2.3. Few-Shot Object Detection

Few-shot object detection (FSOD) aims to recognize novel object categories with limited labeled examples. Early FSOD methods [23] employed meta-learning strategies to transfer knowledge from base to novel classes. FSMOD-Net [14] and Cross-Modality Interaction [8] specifically addressed few-shot learning in multispectral domains through cross-modal feature fusion and semantic prototype alignment. Our work diverges by investigating VLM-based approaches, which offer stronger generalization through semantic grounding.

2.4. Vision-Language Models for Detection

VLMs have revolutionized open-vocabulary object detection by aligning visual representations with semantic embeddings. GLIP [9] unified object detection and phrase grounding through language-image pretraining, enabling zero-shot transfer to novel categories. YOLO-World [2] extended the YOLO architecture with language-conditioned heads for prompt-based adaptation. GroundingDINO [11]

achieved state-of-the-art performance by grounding dynamic object queries in natural language embeddings. These models demonstrate that semantic knowledge from large-scale pretraining can effectively transfer to detection tasks with minimal fine-tuning, motivating our exploration of VLM capabilities in multispectral domains.

3. Methodology

We investigate the potential of VLMs for few-shot multi-spectral object detection through two novel architectures: MS-GDINO and MS-YOLOW. Both models extend VLM principles to multispectral inputs while preserving their language-guided reasoning capabilities. Although they differ in design, transformer-based for MS-GDINO and convolutional for MS-YOLOW, both share a unified philosophy illustrated in Fig. 2. Let $(I_{\text{RGB}}, I_{\text{IR}})$ denote an aligned multispectral image pair and \mathcal{P} the textual prompt describing all target classes (e.g. “person”, “car”, ...). The following sections detail how our framework processes these inputs through complementary visual and textual pathways to achieve robust multispectral detection.

3.1. Dual-Modality Visual Encoding

We extract multi-scale feature maps from aligned RGB and IR inputs using modality-specific backbones (Sec. 4):

$$\{F_{\text{RGB}}^1, \dots, F_{\text{RGB}}^L\} = \text{Backbone}_{\text{RGB}}(I_{\text{RGB}}), \quad (1)$$

$$\{F_{\text{IR}}^1, \dots, F_{\text{IR}}^L\} = \text{Backbone}_{\text{IR}}(I_{\text{IR}}), \quad (2)$$

where $F_m^l \in \mathbb{R}^{C_l \times H_l \times W_l}$ is the feature map of modality $m \in \{\text{RGB}, \text{IR}\}$ at level l with C_l channels and spatial dimensions $H_l \times W_l$. We denote the multi-scale features of each modality by $\mathcal{F}_m = \{F_m^1, \dots, F_m^L\}$, which serve as inputs to the detection heads.

3.2. Textual Representation Encoding

The prompt is embedded through a pretrained language encoder such as BERT [4] or CLIP [16]:

$$T = \text{TextEncoder}(\mathcal{P}) \in \mathbb{R}^{N_t \times d}, \quad (3)$$

where N_t is the number of tokens in the prompt and d is the model dimensionality. The embeddings act as category queries, enabling the model to associate image regions with textual semantics even for unseen categories.

3.3. Spectral Feature Enhancement

We process the multi-scale features of each modality through separate vision-language encoders to preserve and enhance modality-specific representations:

$$\mathcal{F}'_{\text{RGB}}, T'_{\text{RGB}} = \text{Encoder}_{\text{RGB}}(\mathcal{F}_{\text{RGB}}, T), \quad (4)$$

$$\mathcal{F}'_{\text{IR}}, T'_{\text{IR}} = \text{Encoder}_{\text{IR}}(\mathcal{F}_{\text{IR}}, T). \quad (5)$$

This design choice, as opposed to using a single shared module, allows each modality to develop specialized representations while leveraging the inherent cross-spectral generalization capabilities of VLMs. This results in enhanced visual features \mathcal{F}'_m with integrated semantic context and modality-conditioned text features T'_m adapted to spectral characteristics.

3.4. Prediction Head

The prediction head converts fused multispectral visual features and modality-specific text embeddings into final bounding boxes and class scores. Both MS-GDINO and MS-YOLOW follow the same fusion principle: visual features are summed across modalities and text embeddings are concatenated, while class logits are obtained by taking the element-wise maximum across modality-specific similarity scores. We define the fused visual map and fused text embedding as:

$$\mathbf{F}_{\text{fused}} = \mathcal{F}'_{\text{RGB}} + \mathcal{F}'_{\text{IR}}, \quad (6)$$

$$\mathbf{T}_{\text{fused}} = \text{Concat}(T'_{\text{RGB}}, T'_{\text{IR}}). \quad (7)$$

3.4.1. MS-GDINO

Multispectral Language-guided query selection MS-GDINO explicitly selects spatial positions to form object queries using cross-modal semantic affinity. After feature enhancement, the goal is to extract a set of N_q informative object queries that will serve as input to a decoder. For each modality m , we compute semantic affinity matrices between enhanced visual tokens and updated text tokens as a dot-product:

$$S_m = \mathcal{F}'_m \cdot (T'_m)^\top. \quad (8)$$

The affinity matrices from both modalities are concatenated along the spatial dimension:

$$S = \text{Concat}(S_{\text{RGB}}, S_{\text{IR}}). \quad (9)$$

Finally, the top- N_q visual positions are selected based on the maximum similarity along the text dimension:

$$\mathcal{I}_{N_q} = \text{Top}_{N_q} \left(\max^{(-1)}(S) \right), \quad (10)$$

where $\max^{(-1)}(\cdot)$ denotes the maximum operation along the text dimension. This selection strategy ensures that the decoder receives the most discriminative queries from either modality, prioritized by their semantic relevance to the text descriptions. The features at \mathcal{I}_{N_q} are used to form the initial object queries $\mathbf{Q}_0 \in \mathbb{R}^{N_q \times d}$ supplied to the transformer decoder.

Cross-modality decoder MS-GDINO refines the selected queries via a cross-modality transformer decoder. The decoder iteratively updates query embeddings \mathbf{Q}_j for $j = 1, \dots, J$ using self-attention, cross-attention to visual

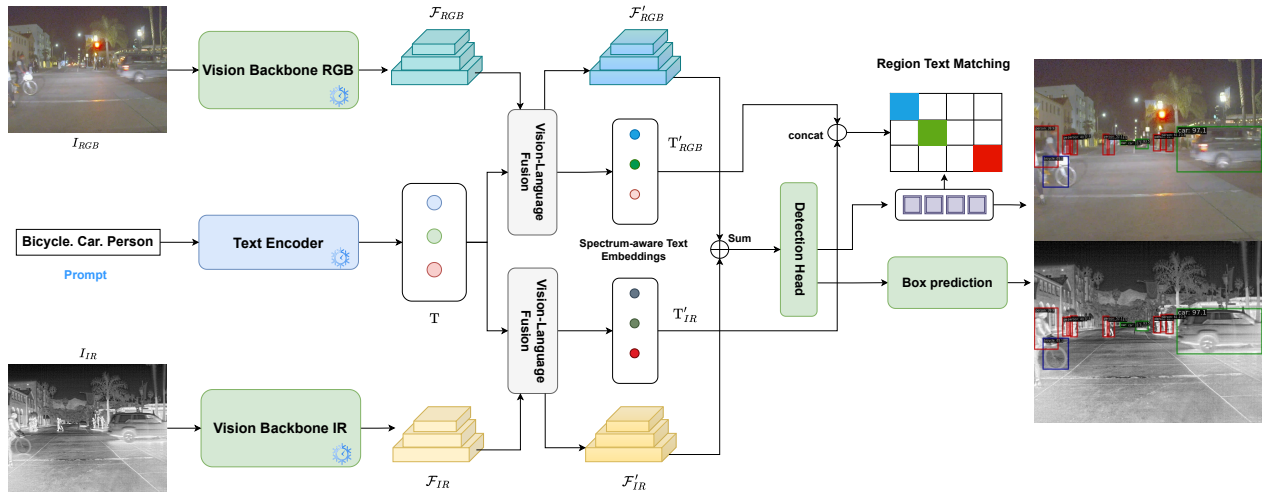


Figure 2. Overall architecture of MS-X instantiated using either **Grounding DINO (MS-GDINO)** or **YOLO-World (MS-YOLOW)**. The model processes RGB and IR inputs through separate backbones and encoders, with fusion occurring at the query selection and decoder stages. Text embeddings provide semantic guidance throughout the pipeline.

features, cross-attention to text embeddings, and a feed-forward network:

$$\mathbf{Q}_j^{(1)} = \text{SelfAttn}(\mathbf{Q}_{j-1}) + \mathbf{Q}_{j-1}, \quad (11)$$

$$\mathbf{Q}_j^{(2)} = \text{CrossAttn}(\mathbf{Q}_j^{(1)}, \mathbf{F}_{\text{fused}}) + \mathbf{Q}_j^{(1)}, \quad (12)$$

$$\mathbf{Q}_j^{(3)} = \text{CrossAttn}(\mathbf{Q}_j^{(2)}, \mathbf{T}_{\text{fused}}) + \mathbf{Q}_j^{(2)}, \quad (13)$$

$$\mathbf{Q}_j = \text{FFN}(\mathbf{Q}_j^{(3)}) + \mathbf{Q}_j^{(3)}. \quad (14)$$

The final queries $\mathbf{Q}_{\text{out}} \in \mathbb{R}^{N_q \times d}$ are projected to bounding boxes and class logits. Bounding boxes are regressed via a MLP,

$$\hat{\mathbf{b}} = \text{MLP}_{\text{box}}(\mathbf{Q}_{\text{out}}) \in \mathbb{R}^{N_q \times 4}, \quad (15)$$

and class logits are obtained by measuring similarity between decoder outputs and each modality’s text embeddings and then taking an element-wise maximum across modalities:

$$\hat{\mathbf{p}} = \max_{m \in \{\text{RGB}, \text{IR}\}} (\mathbf{Q}_{\text{out}} \cdot (\mathbf{T}'_m)^\top) \in \mathbb{R}^{N_q \times N_t}. \quad (16)$$

The max is applied element-wise across the modality dimension so that the strongest modality-driven logit is preserved for each class and query.

3.4.2. MS-YOLOW

MS-YOLOW performs detection directly on multi-scale fused feature maps $\mathbf{F}_{\text{fused}}$ without explicit object queries. A lightweight convolutional stack processes features at multiple scales to produce detection outputs. At each feature

level, bounding boxes are regressed through dedicated convolutional layers:

$$\hat{\mathbf{b}}^l = \text{Conv}_{\text{box}}(\mathbf{F}_{\text{fused}}^l) \in \mathbb{R}^{H_l \times W_l \times 4}, \quad (17)$$

where l indexes the feature pyramid levels with spatial dimensions $H_l \times W_l$. Class logits are computed by measuring similarity between multi-scale visual features and text embeddings:

$$\ell_m^l = \mathbf{F}_{\text{fused}}^l \cdot (\mathbf{T}'_m)^\top, \quad m \in \{\text{RGB}, \text{IR}\}, \quad (18)$$

and aggregated across modalities via element-wise maximum:

$$\hat{\mathbf{p}}^l = \max_{m \in \{\text{RGB}, \text{IR}\}} \ell_m^l \in \mathbb{R}^{H_l \times W_l \times N_t}. \quad (19)$$

4. Experiments

We present extensive experimental validation of the proposed framework, focusing on its few-shot learning capabilities to address practical data scarcity challenges. To provide context and establish upper-bound performance, we also evaluate the model using all available annotations, enabling comparison with state-of-the-art approaches. This comprehensive evaluation highlights the framework’s effectiveness in low-data regimes while demonstrating competitive performance when abundant annotations are accessible.

4.1. Datasets

Our evaluation employs two challenging multispectral benchmarks that provide precisely aligned RGB-IR image pairs under diverse environmental conditions.

Shots	Method	Spectrum	Backbone	Bicycle	Car	Person	All
5-shot	DAMSDet	RGB+IR	Resnet50	36.40	43.16	42.34	40.63
	CAFF-DINO	RGB+IR	Resnet50	18.00	40.30	25.20	27.83
	YOLOW-M	RGB	CSPDarknet	41.41	67.84	55.70	54.98
	YOLOW-M	IR	CSPDarknet	53.42	<u>78.56</u>	76.80	69.59
	MS-YOLOW-M (Ours)	RGB+IR	CSPDarknet	58.00	79.01	<u>75.05</u>	70.69
	GDINO-T	RGB	SwinT	44.17	66.93	58.37	56.49
	GDINO-T	IR	SwinT	51.96	72.13	70.07	64.72
	MS-GDINO-T (Ours)	RGB+IR	SwinT	<u>57.63</u>	78.37	73.67	<u>69.88</u>
10-shot	DAMSDet	RGB+IR	Resnet50	39.69	50.31	52.19	47.40
	CAFF-DINO	RGB+IR	Resnet50	24.30	40.50	31.90	32.23
	YOLOW-M	RGB	CSPDarknet	42.57	67.79	55.66	55.34
	YOLOW-M	IR	CSPDarknet	54.08	78.53	76.74	69.78
	MS-YOLOW-M (Ours)	RGB+IR	CSPDarknet	59.37	79.58	<u>74.60</u>	71.15
	GDINO-T	RGB	SwinT	43.22	69.66	60.52	57.80
	GDINO-T	IR	SwinT	46.22	74.49	71.74	64.15
	MS-GDINO-T (Ours)	RGB+IR	SwinT	<u>57.86</u>	<u>78.89</u>	73.97	<u>70.25</u>

Table 1. Few-shot object detection results on the FLIR dataset under different shot settings. The ‘‘All’’ column reports the mAP50 across all classes. For each setting the best and second-best results are highlighted in **bold** and underline, respectively.

FLIR [20] comprises synchronized RGB-thermal image pairs captured in automotive scenarios. We use the aligned version of the dataset from [24] containing 4,129 training and 1,013 testing image pairs. It covers 3 classes *person*, *car* and *bicycle*. The thermal modality exhibits a resolution of 640×512 pixels. semantically distinct categories: *person*, *car*, and *bicycle*.

M3FD [10] contains 4,200 co-registered RGB-thermal pairs captured across diverse conditions including Day, Night, Overcast, and Challenge scenarios. The annotations cover six object categories: *person*, *car*, *truck*, *bus*, *motorcycle*, and *traffic light*. As no official public split is available, we adopt the dataset partition provided by [5] to ensure fair comparison with existing methods.

4.2. Few-Shot Learning Protocol

To evaluate the framework’s data-efficient learning capabilities, we adopt the few-shot detection benchmark established by FSMODNet [14]. This benchmark provides standardized few-shot splits for multispectral datasets, ensuring fair comparison across methods. For each dataset and object category, we utilize the predefined support sets containing k annotated instances, where $k \in \{5, 10\}$. Models are trained exclusively on these support samples and evaluated on the complete test set. For comprehensive evaluation, we compare against three state-of-the-art multispectral object detectors: DAMSDet [5], CAFF-DINO [6], and GM-DETR [21]. To enable a fair comparison, we initialize all baseline models with COCO pre-trained weights and fine-tune them on the target multispectral datasets using the official code, unlike [14], where models were trained from scratch.

4.3. Evaluation Metrics

Detection performance is quantified using established metrics appropriate for each experimental setting. For few-shot evaluation, we report mean Average Precision at IoU threshold 0.50 (mAP50), which provides a robust measure of detection accuracy in low-data regimes. Fully supervised experiments employ the comprehensive COCO evaluation suite: mAP, mAP50, and mAP75.

4.4. Implementation Details

All experiments are implemented using the MMDetection [1] and MMYOLO [3] codebases built on PyTorch, and trained on NVIDIA A100 GPUs. Both visual backbones and text encoders are kept frozen during training to maintain the integrity of pre-trained representations and prevent overfitting in few-shot scenarios. During inference, we evaluate models at a single resolution of 640×640 without test-time augmentation to ensure fair comparison and computational efficiency.

Few-Shot Training In the few-shot regime, we train our models for 50 epochs with an initial learning rate of 1×10^{-5} for MS-GDINO and 5×10^{-5} for MS-YOLOW. We use the **Tiny** variant for Grounding DINO and the **Medium** variant of YOLOW as bigger models were subject to severe overfitting in early experiments. Each experiment is repeated ten times with different random seeds, and the average score is reported to account for variance due to random sampling.

Pseudo-Labeling Few-shot object detection suffers from *incomplete supervision*, where many valid objects remain unlabeled because only a few instances per class are annotated. This issue is particularly severe in multispectral and

densely populated datasets such as FLIR and M3FD. Training a VLM on such data implicitly teaches the model to interpret unlabeled objects as background, introducing *false-negative supervision* that reduces recall and harms generalization. To alleviate this, we employ a *pseudo-labeling* strategy to enrich the sparse annotations. For each image, let \mathcal{G} denote its set of ground-truth boxes, and let the model generate candidate detections $\{(b_j, s_j, c_j)\}_j$ (box, score, class), retaining only those above an adaptive threshold:

$$\tau = \max(\mu + \sigma, \tau_{\text{floor}}), \quad (20)$$

where μ and σ denote the mean and standard deviation of detection scores $\{s_j\}$ for the image. The lower bound of τ_{floor} prevents low-confidence predictions from contaminating the pseudo-label set when the model is uncertain. We found in ablations (Sec. 5.4) that the value of 0.35 works well in practice. After applying class-specific non-maximum suppression (NMS), a candidate (b_j, s_j, c_j) is accepted as a pseudo-label only if it does not significantly overlap any ground-truth box of the same class:

$$\max_{\substack{g \in \mathcal{G} \\ \text{class}(g)=c_j}} \text{IoU}(b_j, g) < \delta, \quad (21)$$

where we set $\delta = 0.3$ empirically. Accepted pseudo-labels are merged with the original annotations and used as additional positives during training. This procedure allows the model to recover missing annotations, leveraging its zero-shot detection ability while keeping pseudo-label noise minimal.

5. Results

5.1. Few-Shot Multispectral Object Detection

Results on the FLIR Dataset Tab. 1 summarizes performance on FLIR. Across all few-shot regimes, both multispectral variants significantly outperform their unimodal counterparts. In the 5-shot setting, **MS-YOLOW** achieves a mAP of **70.69%**, outperforming YOLOW-M (RGB) and YOLOW-M (IR) by **+15.71%** and **+1.10%**, respectively. Similarly, **MS-GDINO** reaches **69.88%**, improving upon GDINO (RGB) by **+13.39%** and GDINO (IR) by **+1.49%**. The findings indicate that leveraging complementary spectral cues enhances detection accuracy across classes, with a great impact in few-shot scenarios where unimodal models often overfit. Extended 30-shot experiments are reported in the supplementary material (Sec. 8.1).

Results on the M3FD Dataset We next evaluate on the M3FD dataset (Tab. 2), which introduces a more diverse set of urban traffic categories and illumination variations. The trends are consistent with those observed on FLIR: our multispectral detectors clearly outperform unimodal baselines. In the 5-shot configuration, **MS-GDINO** achieves

66.33% mAP, a relative improvement of **+3.45%** over GDINO (RGB) and **+24.89%** over GDINO (IR). Likewise, **MS-YOLOW** surpasses YOLOW (RGB) by **+2.73%** and YOLOW-M (IR) by a large margin of **+22.24%**. When scaling to 10-shot training, **MS-GDINO** achieves the best overall mAP of **67.01%**, reaffirming the effectiveness of multispectral grounding even within VLMs. The substantial and consistent gains across modalities, detectors, and datasets indicate that the proposed approach generalizes well to heterogeneous spectral distributions and challenging environmental conditions. We include further qualitative comparisons and failure cases in the supplementary material (Sec. 9).

Progressive Improvements Both MS-YOLOW and MS-GDINO exhibit consistent gains when increasing the annotation budget from 5-shot to 10-shot. On FLIR (Tab. 1), MS-YOLOW improves from 70.69 to 71.15 mAP₅₀ (+0.46), while MS-GDINO rises from 69.88 to 70.25 (+0.37). On M3FD (Tab. 2), MS-YOLOW increases from 62.19 to 62.69 (+0.50) and MS-GDINO from 66.33 to 67.01 (+0.68). These gains, though moderate, are consistent across frameworks and datasets, reflecting two complementary factors. First, our pseudo-labeling strategy effectively amplifies supervision: high-confidence pseudo-annotations increase sample diversity and coverage, particularly for underrepresented classes or challenging viewpoints. Second, the pretrained vision-language backbones provide strong transferable features, which saturate in few-shot regimes; additional labels produce stable, incremental improvements rather than large jumps, highlighting the robustness of the models to low-data scenarios. Overall, the results demonstrate that both frameworks benefit from additional supervision, achieving reliable, steady improvements while maintaining stability and avoiding overfitting.

5.2. Upper-Bound Training and Scalability

Although our primary focus lies in few-shot and data-limited multispectral object detection, we also evaluate our frameworks under full supervision to assess their upper-bound performance and scalability. In this setting, we further explore larger model variants to examine how capacity influences multispectral fusion and language-guided detection. This analysis reveals how the proposed architectures behave when ample annotated data and higher model capacity are available. Tabs. 4 and 5 summarize the results on the FLIR and M3FD benchmarks. We compare our frameworks against recent state-of-the-art multispectral detectors, including DAMSDet [5], Fusion-Mamba [22], and CAFF-DINO [6]. Our experiments reveal several key insights. First, both frameworks demonstrate excellent scalability with model capacity, showing consistent performance improvements as the backbone transitions from Swin-T to Swin-L. On the FLIR dataset, MS-GDINO (Swin-L)

Shots	Method	Spectrum	Backbone	Person	Car	Bus	Motorcycle	Traffic Light	Truck	All
5-shot	DAMSDet	RGB+IR	Resnet50	13.26	36.12	30.36	27.39	25.81	34.23	27.86
	CAFF-DINO	RGB+IR	Resnet50	8.21	31.92	35.56	18.56	8.92	31.68	22.48
	YOLOW-M	RGB	CSPDarknet	44.50	83.70	68.63	64.43	<u>51.70</u>	72.57	<u>64.92</u>
	YOLOW-M	IR	CSPDarknet	47.47	57.00	56.87	31.47	12.83	30.03	39.95
	MS-YOLOW-M (Ours)	RGB+IR	CSPDarknet	<u>52.36</u>	<u>84.81</u>	70.59	58.01	46.63	60.73	62.19
	GDINO-T	RGB	SwinT	45.57	73.79	72.97	<u>67.26</u>	59.70	57.96	62.88
	GDINO-T	IR	SwinT	46.44	58.89	56.56	36.06	16.62	34.07	41.44
	MS-GDINO-T (Ours)	RGB+IR	SwinT	55.16	86.11	<u>71.86</u>	70.64	51.46	<u>62.73</u>	66.33
10-shot	DAMSDet	RGB+IR	Resnet50	18.15	46.07	47.81	45.82	29.15	42.02	38.17
	CAFF-DINO	RGB+IR	Resnet50	10.84	31.62	51.51	29.66	12.74	37.17	28.92
	YOLOW-M	RGB	CSPDarknet	44.50	76.90	70.70	65.18	50.12	66.21	62.27
	YOLOW-M	IR	CSPDarknet	47.47	56.96	58.82	34.02	15.15	32.75	40.86
	MS-YOLOW-M (Ours)	RGB+IR	CSPDarknet	<u>52.36</u>	<u>78.52</u>	72.99	59.89	46.05	56.51	62.69
	GDINO-T	RGB	SwinT	45.43	73.90	75.54	<u>67.15</u>	57.29	60.18	<u>63.58</u>
	GDINO-T	IR	SwinT	46.48	60.49	60.76	38.24	19.50	40.25	44.62
	MS-GDINO-T (Ours)	RGB+IR	SwinT	55.20	85.78	<u>73.40</u>	70.96	54.64	<u>63.43</u>	67.01

Table 2. Few-shot object detection results on the M3FD dataset under varying shot settings. The ‘‘All’’ column reports the mAP50 across all classes. For each setting the best and second-best results are highlighted in **bold** and underline, respectively.

achieves a new state-of-the-art mAP of 50.5, outperforming DAMSDet (49.3) and Fusion-Mamba (47.0). Similarly, on the M3FD dataset, YOLOW-L achieves 48.7 mAP, while MS-GDINO (Swin-L) reaches 55.3 mAP, surpassing prior methods by a significant margin. These results confirm that our framework not only generalizes well in few-shot settings but also scales effectively when fully supervised.

5.3. From Zero-shot to Few-shot

We analyze the performance progression from mono-spectral zero-shot baselines to multispectral few-shot learning for both frameworks, demonstrating how each effectively leverages limited annotations across spectral modalities. Tab. 3 shows interesting patterns across both frameworks in the zero-shot to few-shot setting. Both frameworks demonstrate significant performance gains through multispectral fusion in few-shot settings. MS-YOLOW achieves 70.69 mAP50 in the 5-shot regime, surpassing its best mono-spectral zero-shot performance of 69.2 mAP50. Similarly, MS-GDINO reaches 69.88 mAP50 with 5-shot learning, exceeding its top mono-spectral zero-shot result of 65.3 mAP50. This demonstrates that multispectral fusion provides immediate performance benefits over even the strongest individual modalities, validating the complementary nature of RGB and infrared information for multispectral object detection.

5.4. Effect of the Confidence Floor (τ_{floor})

We examine how the pseudo-labeling floor τ_{floor} impacts the number and reliability of generated pseudo-labels and consequently the few-shot fine-tuning performance. This parameter effectively serves as a bias-variance control: lower values increase recall by allowing more detections to be

Dataset	Setting	Model	Spectrum	mAP50
FLIR	Zero-shot	YOLOW-M	RGB	55.2
		YOLOW-M	IR	69.2
		GDINO-T	RGB	54.2
		GDINO-T	IR	65.0
	5-shot	MS-YOLOW-M	RGB+IR	70.68
		MS-GDINO-T	RGB+IR	69.89
M3FD	Zero-shot	YOLOW-M	RGB	63.4
		YOLOW-M	IR	35.5
		GDINO-T	RGB	61.9
		GDINO-T	IR	34.5
	5-shot	MS-YOLOW-M	RGB+IR	62.19
		MS-GDINO-T	RGB+IR	66.33

Table 3. Performance on FLIR and M3FD datasets under zero-shot and few-shot (5-shot) settings for both MS-YOLOW and MS-GDINO frameworks.

added as pseudo-labels, while higher values improve precision by filtering out uncertain predictions. To quantify this trade-off, we vary τ_{floor} in the range $[0.2, 1.0]$. As shown in Tab. 6, moderate floor values around $\tau_{\text{floor}}=0.35$ achieve the best overall performance, improving mAP50 by roughly +2 points compared to the no-pseudo-label baseline ($\tau_{\text{floor}}=1.0$). Lowering the floor to 0.2 slightly increases recall but introduces noisy pseudo-labels that degrade performance. For high-frequency classes like *Person* and *Car*, such a low threshold maximizes mAP50 by including moderate-confidence true positives, boosting effective training data while adding minimal noise. On the other hand, moderately difficult or ambiguous classes like *Traffic light* and *Motorcycle* require higher thresholds ($\tau_{\text{floor}} = 0.5$) to preserve precision and avoid incorrect pseudo-labels that

Method	mAP	mAP50	mAP75
CFT [15]	40.2	78.7	35.5
ICAFusion [19]	41.4	79.2	36.9
YOLOXCPCF [7]	44.6	82.1	41.2
CAFF-DINO* [6]	45.6	83.1	42.3
GMDETR [21]	45.8	83.9	42.6
DAMSDet [5]	49.3	<u>86.6</u>	48.1
Fusion-Mamba [22]	47.0	84.9	45.9
MS-YOLOW-M	47.8	83.5	45.9
MS-YOLOW-L	48.9	85.3	47.7
MS-GDINO-T	48.5	86.0	47.6
MS-GDINO-B	<u>49.4</u>	85.9	<u>49.2</u>
MS-GDINO-L	50.5	87.8	51.3

Table 4. Comparison with state-of-the-art methods on the FLIR dataset. Model variants: **M** (Medium), **L** (Large), **T** (Tiny), **B** (Base). Note: CAFF-DINO* results were originally reported with 800×1000 resolution and have been re-evaluated at 640×640 for fair comparison. The best and second-best results are highlighted in **bold** and underline, respectively.

Method	mAP	mAP50	mAP75
CFT [15]	42.5	68.2	44.6
ICAFusion [19]	41.9	67.8	44.5
DAMSDet [5]	<u>52.9</u>	80.2	56.0
CAFF-DINO [6]	49.0	75.5	52.7
MS-YOLOW-M	48.4	72.8	51.3
MS-YOLOW-L	48.7	73.0	51.1
MS-GDINO-T	50.6	79.0	53.5
MS-GDINO-B	52.5	<u>80.7</u>	<u>56.1</u>
MS-GDINO-L	55.3	83.3	58.4

Table 5. Comparison with state-of-the-art methods on M3FD dataset. Model variants: **M** (Medium), **L** (Large), **T** (Tiny), **B** (Base). The best and second-best results are highlighted in **bold** and underline, respectively.

τ_{floor}	Person	Car	Bus	Motorcycle	Traffic light	Truck	All
0.20	55.3	86.5	69.2	68.9	46.9	60.9	64.6
0.35	55.2	86.1	71.7	70.6	51.5	62.7	66.3
0.50	51.6	82.0	70.9	65.9	53.0	62	64.3
0.75	47.6	72.8	66.3	60.7	50.7	50.0	57.7
1.00	46.3	71.4	69.7	58.6	50.0	50.0	57.7

Table 6. Effect of the pseudo-labeling floor τ_{floor} on few-shot detection (5-shot regime) for MS-GDINO on M3FD. Per-class mAP50 and overall mAP50 are reported.

harm few-shot learning.

5.5. Runtime analysis

Tab. 7 reveals substantial benefits of multispectral fusion with distinct efficiency-accuracy trade-offs. Mono-spectral RGB baselines show limited performance (22.9-

25.3 mAP), demonstrating the fundamental challenge of single-modality detection. The transition to multispectral processing yields dramatic improvements: MS-YOLOW-M achieves +24.9 mAP over its mono-spectral counterpart while maintaining real-time performance (27.9 FPS). YOLOW variants demonstrate superior computational efficiency, with MS-YOLOW-M achieving 27.9 FPS—approximately 3× faster than MS-GDINO-T (8.8 FPS) and 10× faster than MS-GDINO-L (2.6 FPS). However, MS-GDINO-L achieves the best detection performance with 50.5 mAP and 87.8 mAP50, representing a +25.2 mAP improvement over its mono-spectral baseline. This analysis reveals clear deployment guidelines: MS-YOLOW for real-time applications requiring efficiency, and MS-GDINO for accuracy-critical scenarios. Both multispectral approaches substantially outperform mono-spectral counterparts, validating our core premise.

Model	Spec.	Params (M)	FPS	mAP	mAP50
YOLOW-M	RGB	92	31.6	22.9	55.2
YOLOW-L	RGB	110	28.2	23.2	55.6
GDINO-T	RGB	172	11.9	22.6	55.2
GDINO-L	RGB	341	3.5	25.3	60.2
MS-YOLOW-M	RGB+IR	104	27.9	47.8	83.5
MS-YOLOW-L	RGB+IR	131	24.0	<u>48.9</u>	85.3
MS-GDINO-T	RGB+IR	198	8.8	48.5	<u>86.0</u>
MS-GDINO-L	RGB+IR	367	2.6	50.5	87.8

Table 7. Runtime and detection performance on FLIR using an A100 GPU at 640×640 input. Best and second-best are in **bold** and underline.

6. Conclusion and Future Work

In this work, we presented the first systematic study of VLMs for few-shot multispectral object detection, bridging the gap between language-grounded pretraining and multispectral perception. By introducing lightweight adaptations of **Grounding DINO** and **YOLO-World**, we demonstrated that semantic priors learned from large-scale image-text data effectively transfer across spectral domains, substantially improving data efficiency and robustness. Extensive experiments on the FLIR and M3FD benchmarks established new state-of-the-art results in both few-shot and fully supervised regimes, while further experiments revealed that adaptive pseudo-labeling and simple fusion mechanisms are sufficient to unlock strong cross-spectral generalization. Our findings highlight that semantic grounding, rather than complex fusion, is the key to robust multispectral learning. The success of VLMs in this setting suggests that modality-agnostic semantic spaces learned from web-scale data can serve as universal representations for heterogeneous sensor modalities. A promising direction of research is to study the **zero-shot adaptability of VLMs to rare or unseen**

classes in multispectral domains, as current datasets primarily contain common categories such as *person* and *car*. Evaluating and improving transfer to uncommon or fine-grained categories would provide deeper insight into the limits of semantic generalization across wavelengths.

References

- [1] Kai Chen, Jiaqi Wang, Jiangmiao Pang, Yuhang Cao, Yu Xiong, Xiaoxiao Li, Shuyang Sun, Wansen Feng, Ziwei Liu, Jiarui Xu, Zheng Zhang, Dazhi Cheng, Chenchen Zhu, Tianheng Cheng, Qijie Zhao, Buyu Li, Xin Lu, Rui Zhu, Yue Wu, Jifeng Dai, Jingdong Wang, Jianping Shi, Wanli Ouyang, Chen Change Loy, and Dahua Lin. MMDetection: Open mmlab detection toolbox and benchmark. *arXiv preprint arXiv:1906.07155*, 2019. 5
- [2] Tianheng Cheng, Lin Song, Yixiao Ge, Wenyu Liu, Xinggang Wang, and Ying Shan. Yolo-world: Real-time open-vocabulary object detection. In *Proceedings of the IEEE/CVF conference on computer vision and pattern recognition*, pages 16901–16911, 2024. 2
- [3] MMYOLO Contributors. MMYOLO: OpenMMLab YOLO series toolbox and benchmark. <https://github.com/open-mmlab/mmyolo>, 2022. 5
- [4] Jacob Devlin, Ming-Wei Chang, Kenton Lee, and Kristina Toutanova. Bert: Pre-training of deep bidirectional transformers for language understanding. In *Proceedings of the 2019 Conference of the North American Chapter of the Association for Computational Linguistics (NAACL-HLT)*, pages 4171–4186. Association for Computational Linguistics, 2019. 3
- [5] Junjie Guo, Chenqiang Gao, Fangcen Liu, Deyu Meng, and Xinbo Gao. DAMSDet: Dynamic adaptive multispectral detection transformer with competitive query selection and adaptive feature fusion. In *European Conference on Computer Vision*, pages 464–481. Springer, 2025. 2, 5, 6, 8
- [6] Kevin Helvig, Baptiste Abeloos, and Pauline Trouvé-Peloux. CAFF-DINO: Multi-spectral object detection transformers with cross-attention features fusion. In *Proceedings of CVPR*, pages 3037–3046, 2024. 2, 5, 6, 8
- [7] Sijie Hu, Fabien Bonardi, Samia Bouchafa, Helmut Prendinger, and Désiré Sidibé. Rethinking self-attention for multispectral object detection. *IEEE Transactions on Intelligent Transportation Systems*, 25(11):16300–16311, 2024. 8
- [8] Lian Huang, Zongju Peng, Fen Chen, Shaosheng Dai, Ziqiang He, and Kesheng Liu. Cross-modality interaction for few-shot multispectral object detection with semantic knowledge. *Neural Networks*, 173:106156, 2024. 2
- [9] Liunian Harold Li, Pengchuan Zhang, Haotian Zhang, Jianwei Yang, Chunyuan Li, Yiwu Zhong, Lijuan Wang, Lu Yuan, Lei Zhang, Jenq-Neng Hwang, et al. Grounded language-image pre-training. In *Proceedings of the IEEE/CVF conference on computer vision and pattern recognition*, pages 10965–10975, 2022. 2
- [10] Jian Liu, Xingran Fan, Zhen Huang, Guoliang Wu, Rong Liu, Wei Zhong, and Zhengkai Luo. Target-aware dual adversarial learning and a multi-scenario multi-modality benchmark to fuse infrared and visible for object detection. In *Proceedings of the IEEE/CVF Conference on Computer Vision and Pattern Recognition (CVPR)*, 2023. 5
- [11] Shilong Liu, Zhaoyang Zeng, Tianhe Ren, Feng Li, Hao Zhang, Jie Yang, Qing Jiang, Chunyuan Li, Jianwei Yang, Hang Su, et al. Grounding dino: Marrying dino with grounded pre-training for open-set object detection. In *European conference on computer vision*, pages 38–55. Springer, 2024. 2
- [12] Wei Liu, Dragomir Anguelov, Dumitru Erhan, Christian Szegedy, Scott Reed, Cheng-Yang Fu, and Alexander C. Berg. Ssd: Single shot multibox detector. In *European Conference on Computer Vision (ECCV)*, pages 21–37, 2016. 2
- [13] Anish Madan, Neehar Peri, Shu Kong, and Deva Ramanan. Revisiting few-shot object detection with vision-language models. In *Proceedings of the 38th Conference on Neural Information Processing Systems (NeurIPS 2024), Datasets and Benchmarks Track*, 2024. 2
- [14] Manuel Nkegoum, Minh-Tan Pham, Éliisa Fromont, Bruno Avignon, and Sébastien Lefèvre. Fsmoynet: A closer look at few-shot detection in multispectral data. *arXiv preprint arXiv:2509.20905*, 2025. 2, 5
- [15] Fang Qingyun, Han Dapeng, and Wang Zhaokui. Cross-modality fusion transformer for multispectral object detection. *arXiv preprint arXiv:2111.00273*, 2021. 8
- [16] Alec Radford, Jong Wook Kim, Chris Hallacy, Aditya Ramesh, Gabriel Goh, Sandhini Agarwal, Girish Sastry, Amanda Askell, Pamela Mishkin, Jack Clark, et al. Learning transferable visual models from natural language supervision. In *International conference on machine learning*, pages 8748–8763. PmlR, 2021. 3
- [17] Joseph Redmon, Santosh Divvala, Ross Girshick, and Ali Farhadi. You only look once: Unified, real-time object detection. In *Proceedings of the IEEE Conference on Computer Vision and Pattern Recognition (CVPR)*, pages 779–788, 2016. 2
- [18] Shaoqing Ren, Kaiming He, Ross Girshick, and Jian Sun. Faster R-CNN: Towards real-time object detection with region proposal networks. In *Advances in Neural Information Processing Systems (NeurIPS)*, pages 91–99, 2015. 2
- [19] Jifeng Shen, Yifei Chen, Yue Liu, Xin Zuo, Heng Fan, and Wankou Yang. Icafusion: Iterative cross-attention guided feature fusion for multispectral object detection. *Pattern Recognition*, page 109913, 2023. 8
- [20] FLIR Systems. FLIR thermal dataset, 2019. <https://www.flir.com/oem/adas/adas-dataset-form/>. 5
- [21] Yiming Xiao, Fanman Meng, Qingbo Wu, Linfeng Xu, Mingzhou He, and Hongliang Li. Gm-detr: Generalized multispectral detection transformer with efficient fusion encoder for visible-infrared detection. In *Proceedings of the IEEE/CVF Conference on Computer Vision and Pattern Recognition*, pages 5541–5549, 2024. 2, 5, 8
- [22] Xinyu Xie, Yawen Cui, Tao Tan, Xubin Zheng, and Zitong Yu. Fusionmamba: Dynamic feature enhancement for multi-modal image fusion with mamba. *Visual Intelligence*, 2(37), 2024. 6, 8

- [23] Xiaopeng Yan, Ziliang Chen, Anni Xu, Xiaoxi Wang, Xiaodan Liang, and Liang Lin. Meta R-CNN: Towards general solver for instance-level low-shot learning. In *Proceedings of ICCV*, pages 9577–9586, 2019. [2](#)
- [24] Heng Zhang, Elisa Fromont, Sébastien Lefèvre, and Bruno Avignon. Multispectral fusion for object detection with cyclic fuse-and-refine blocks. In *ICIP 2020 - IEEE International Conference on Image Processing*, pages 1–5, 2020. [5](#)
- [25] Heng Zhang, Elisa Fromont, Sébastien Lefèvre, and Bruno Avignon. Guided attentive feature fusion for multispectral pedestrian detection. In *Proceedings of the IEEE/CVF winter conference on applications of computer vision*, pages 72–80, 2021. [2](#)
- [26] Hao Zhang, Feng Li, Shilong Liu, Lei Zhang, Hang Su, Jun Zhu, Lionel Ni, and Heung-Yeung Shum. DINO: DETR with improved denoising anchor boxes for end-to-end object detection. In *The Eleventh International Conference on Learning Representations*, 2023. [2](#)
- [27] Yian Zhao, Wenyu Lv, Shangliang Xu, Jinman Wei, Guanzhong Wang, Qingqing Dang, Yi Liu, and Jie Chen. DETRs beat YOLOs on real-time object detection. In *Proceedings of the CVPR*, pages 16965–16974, 2024. [2](#)
- [28] Zhuofan Zong, Guanglu Song, and Yu Liu. Detsr with collaborative hybrid assignments training. In *Proceedings of the IEEE/CVF international conference on computer vision*, pages 6748–6758, 2023. [2](#)

From Words to Wavelengths: VLMs for Few-Shot Multispectral Object Detection

Supplementary Material

This supplementary document provides additional details and results complementing the main paper, “*From Words to Wavelengths: VLMs for Few-Shot Multispectral Object Detection.*” We first describe the adaptive pseudo-labelling thresholding strategy used to construct reliable annotations for few-shot learning in Sec. 7. Extended experiments under the 30-shot configuration are presented in Sec. 8.1, supplementing the 5-shot and 10-shot results reported in the main text. We further analyze cross-domain and open-set generalization in multispectral fine-tuning in Sec. 8.2 and include visual examples of detection outputs in Sec. 9. Unless otherwise stated, all experiments follow the same data splits, hyperparameters, and training settings as detailed in the main paper.

7. Pseudo-Labeling threshold

To generate reliable pseudo-labels for augmenting the few-shot datasets, we analyze the confidence calibration of a reference model (Grounding DINO). The goal is to automatically identify high-confidence detections that likely correspond to unlabeled true objects, while filtering out uncertain predictions that could introduce noise. We begin by evaluating the model on the 5-shot training splits of M3FD and collecting the confidence scores of the top-50 predictions per image. As shown in Fig. 3, the overall distribution of prediction scores exhibits a right-skewed pattern, with a high frequency of detections at lower confidence levels (scores ≤ 0.3), indicating that a substantial portion of the model’s predictions are low-confidence and potentially unreliable. The frequency of predictions decreases rapidly as confidence increases, suggesting that high-confidence detections are relatively rare. Fig. 3 also summarizes per-image confidence distributions by showing the median and 75th percentile of the top-50 predictions for each image. For example, if the 75th percentile for an image is 0.3, this means that 38 out of the 50 top predictions have confidence scores below or equal to 0.3, while only the remaining 12 predictions exceed this value. The substantial vertical spread across images indicates dramatic inter-image variability: some images have consistently high-confidence detections, whereas for other images even the top quartile of predictions falls below 0.1 confidence. This variability demonstrates that applying a fixed global confidence threshold would be suboptimal, as the reliability of pseudo-labels depends heavily on individual image content and context. Such under-confidence is consistent with the limited supervision in few-shot settings, where many valid objects

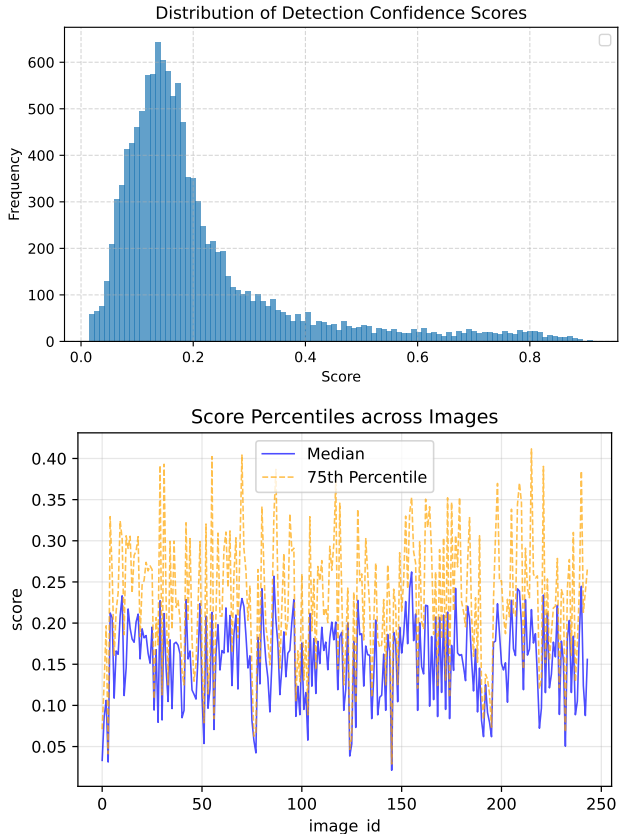


Figure 3. Analysis of detection confidence scores from Grounding DINO on few-shot training splits. **Top:** Histogram of all prediction scores shows a right-skewed distribution with high frequency of low-confidence detections. **Bottom:** Per-image statistics showing median and 75th percentile scores reveal substantial variation across images, with some having consistently high-confidence predictions while others contain predominantly low-scoring detections.

remain unannotated, causing the model to underestimate its detection certainty. As described in the main text, we address this issue using an adaptive thresholding strategy when generating pseudo-labels, selecting high-confidence predictions in a manner tailored to each image’s score distribution. For completeness, we restate the formulation here. For each image, the threshold τ is computed as

$$\tau = \max(\mu + \sigma, \tau_{\text{floor}}),$$

where μ and σ are the mean and standard deviation of the detection scores within that image, and τ_{floor} defines a con-

fidence floor. The adaptive term $\mu + \sigma$ adjusts to local score distributions, promoting higher selectivity for well-calibrated images and tolerance for uncertain ones. The floor τ_{floor} serves as a safety guard, preventing the threshold from collapsing to unreasonably low values when the model is highly uncertain. Pseudo-labels are then selected from detections with $s_j \geq \tau$ and a maximum intersection-over-union (IoU) below 0.3 with any ground-truth annotation of the same class. This ensures that pseudo-labels complement, rather than duplicate, existing annotations. The resulting pseudo-labeled datasets are stored as extended COCO-format annotation files and used for subsequent fine-tuning experiments.

8. Additional Experimental Results

8.1. 30-shot Results

To further analyze performance scaling with increased supervision, we extend our few-shot experiments to the 30-shot regime on both the FLIR and M3FD benchmarks. Results are summarized in Tabs. 2 and 8.

On **FLIR**, both multispectral frameworks exhibit steady improvements compared to their 10-shot counterparts. MS-YOLOW achieves 72.05 mAP₅₀, while MS-GDINO reaches 71.52 mAP₅₀, marking absolute gains of +0.9 and +1.3 points, respectively. Class-wise analysis shows that underrepresented categories such as *Bicycle* benefit the most from additional annotations (+2.95 mAP₅₀ for MS-YOLOW), whereas already saturated classes like *car* and *person* experience marginal but consistent improvements.

A similar trend appears on **M3FD**, where both frameworks maintain strong cross-domain performance. MS-YOLOW improves from 62.69 to 64.44 mAP, while MS-GDINO increases from 67.01 to 67.57 mAP, demonstrating robust scaling despite distributional and spectral shifts. Notably, MS-GDINO continues to excel on complex classes such as *bus* and *motorcycle*, reflecting the advantage of transformer-based multimodal reasoning, whereas MS-YOLOW sustains higher throughput and competitive per-class detection, particularly on *car* and *person*.

Overall, the 30-shot results across both datasets confirm that the proposed multispectral frameworks remain data-efficient and generalizable, with consistent, class-dependent improvements. The incremental gains highlight the complementary strengths of each architecture—YOLOW favoring efficiency and dense supervision, while GDINO excels in semantic grounding and multimodal fusion under low-data conditions.

8.2. Open-Set Generalization in Multispectral Fine-Tuning

Vision–language models naturally support open-set recognition, allowing them to localize categories unseen during

training. A common concern, however, is that domain-specific fine-tuning may reduce this generalization ability by overfitting to the target domain. To examine whether multispectral fine-tuning preserves cross-domain transfer, we fine-tune Grounding DINO on FLIR and evaluate on the unseen M3FD benchmark.

As shown in Tab. 10, the RGB-only zero-shot model obtains 38.9 mAP and 61.9 mAP₅₀ on M3FD, substantially outperforming the IR-only zero-shot model (19.8 mAP, 34.5 mAP₅₀), which suffers from a larger domain gap. With only 5 labeled FLIR images, the multispectral model achieves 38.9 mAP and 63.3 mAP₅₀, matching or slightly surpassing the RGB zero-shot performance. Increasing the supervision to 30 images yields 37.6 mAP and 60.6 mAP₅₀, still close to the zero-shot baseline. In contrast, full-shot fine-tuning reduces performance to 26.5 mAP and 48.4 mAP₅₀, indicating that heavy specialization to FLIR reduces open-set transfer. Overall, these results show that multispectral fine-tuning preserves open-set generalization under low-shot supervision and that the degradation observed under full-shot fine-tuning is primarily due to dataset-specific overfitting rather than catastrophic forgetting. These observations motivate a deeper examination of the zero-shot adaptability of VLMs in multispectral settings, particularly their ability to generalize to object categories that are rare or entirely unseen during fine-tuning.

Setting	Spectrum	mAP	mAP50
Zero-shot transfer	RGB	38.9	61.9
Zero-shot transfer	IR	19.8	34.5
Fine-tuned (FLIR — 5 shot)	RGB + IR	38.9	63.3
Fine-tuned (FLIR — 30 shot)	RGB + IR	37.6	60.6
Fine-tuned (FLIR — full shot)	RGB + IR	26.5	48.4

Table 10. Comparison of Grounding DINO open-set detection performance on M3FD between RGB zero-shot and FLIR fine-tuned models.

9. Visualization of Predictions

We visualize detection results on representative M3FD scenes in Fig. 4. MS-GDINO reliably detects most ground-truth objects across challenging conditions—including low light, distant targets, and crowded scenes—but occasionally produces false positives, such as misidentifying background structures (e.g., predicting a truck instead of a container in the third pair). In contrast, MS-YOLOW behaves more conservatively: it yields fewer false positives but misses several clear objects in crowded or long-range scenarios, as seen in the first pair, although it performs well in low-light scenes. Overall, the qualitative comparison suggests that MS-GDINO favors higher recall at the cost of occasional false alarms, while MS-YOLOW prioritizes

Shots	Method	Spectrum	Backbone	Bicycle	Car	Person	All
10-shot	DAMSDet	RGB+IR	Resnet50	39.69	50.31	52.19	47.40
	CAFF-DINO	RGB+IR	Resnet50	24.30	40.50	31.90	32.23
	YOLOW-M	RGB	CSPDarknet	42.57	67.79	55.66	55.34
	YOLOW-M	IR	CSPDarknet	54.08	78.53	76.74	69.78
	MS-YOLOW-M (Ours)	RGB+IR	CSPDarknet	59.37	79.58	74.60	71.15
	GDINO-T	RGB	SwinT	43.22	69.66	60.52	57.80
	GDINO-T	IR	SwinT	46.22	74.49	71.74	64.15
	MS-GDINO-T (Ours)	RGB+IR	SwinT	57.86	78.89	73.97	70.25
30-shot	DAMSDet	RGB+IR	Resnet50	49.88	58.39	62.98	57.08
	CAFF-DINO	RGB+IR	Resnet50	35.82	51.14	46.42	44.46
	YOLOW-M	RGB	CSPDarknet	46.06	69.72	56.90	57.56
	YOLOW-M	IR	CSPDarknet	55.84	77.70	76.39	69.98
	MS-YOLOW-M (Ours)	RGB+IR	CSPDarknet	62.32	79.16	74.67	72.05
	GDINO-T	RGB	SwinT	49.78	70.53	62.04	60.78
	GDINO-T	IR	SwinT	53.00	76.40	73.44	67.61
	MS-GDINO-T (Ours)	RGB+IR	SwinT	58.86	81.06	74.68	71.52

Table 8. 10-shot and 30-shot object detection results on the FLIR dataset. The 10-shot results, already reported in the main text, are provided here again to facilitate comparison with the 30-shot setting.

Shots	Method	Spectrum	Backbone	Person	Car	Bus	Motorcycle	Traffic Light	Truck	All
10-shot	DAMSDet	RGB+IR	Resnet50	18.15	46.07	47.81	45.82	29.15	42.02	38.17
	CAFF-DINO	RGB+IR	Resnet50	10.84	31.62	51.51	29.66	12.74	37.17	28.92
	YOLOW-M	RGB	CSPDarknet	44.50	76.90	70.70	65.18	50.12	66.21	62.27
	YOLOW-M	IR	CSPDarknet	47.47	56.96	58.82	34.02	15.15	32.75	40.86
	MS-YOLOW-M (Ours)	RGB+IR	CSPDarknet	52.36	78.52	72.99	59.89	46.05	56.51	62.69
	GDINO-T	RGB	SwinT	45.43	73.90	75.54	67.15	57.29	60.18	63.58
	GDINO-T	IR	SwinT	46.48	60.49	60.76	38.24	19.50	40.25	44.62
	MS-GDINO-T (Ours)	RGB+IR	SwinT	55.20	85.78	73.40	70.96	54.64	63.43	67.01
30-shot	DAMSDet	RGB+IR	Resnet50	23.25	56.43	56.39	53.39	38.36	51.52	46.56
	CAFF-DINO	RGB+IR	Resnet50	13.85	40.68	55.82	42.27	20.88	44.62	36.35
	YOLO-World-M	RGB	CSPDarknet	43.63	76.90	70.70	65.18	50.12	66.21	62.12
	YOLO-World-M	IR	CSPDarknet	45.96	56.96	58.82	34.02	15.15	32.75	40.61
	MS-YOLOW-M (Ours)	RGB+IR	CSPDarknet	52.04	85.96	73.24	62.61	49.14	63.04	64.44
	GDINO	RGB	SwinT	45.57	73.79	75.57	67.26	59.70	60.26	63.69
	GDINO	IR	SwinT	46.44	60.56	61.01	38.57	19.76	40.75	44.52
	MS-GDINO-T (Ours)	RGB+IR	SwinT	52.63	85.97	74.10	72.10	53.58	63.43	67.57

Table 9. 10-shot and 30-shot object detection results on M3FD dataset.

precision but struggles with crowded and distant targets.



Figure 4. Qualitative comparison of object detection results on challenging M3FD scenarios. The top part (a) shows the Ground Truth (GT) annotations on the RGB and IR images (first and second line, respectively). The middle part (b) presents the predictions from the MS-GDINO. The bottom part (c) displays the results from MS-YOLOW method. Models were fine-tuned with 5 shots.